

Interval-Based Modeling of High-Temperature Fuel Cells for a Real-Time Control Implementation Under State Constraints

Noël Cont* Wiebke Frenkel* Julia Kersten* Andreas Rauh*
Harald Aschemann*

* *University of Rostock, Chair of Mechatronics,
Justus-von-Liebig-Weg 6, D-18059 Rostock, Germany (e-mail:
contnoel@googlemail.com, {Wiebke.Frenkel, Julia.Kersten,
Andreas.Rauh, Harald.Aschemann}@uni-rostock.de)*

Abstract: Interval-based state estimation techniques represent promising approaches for the quantification of worst-case bounds of those sets of state variables that are reachable over a finitely long time horizon under the consideration of bounded uncertainty. In previous work, it has been shown that such estimation techniques cannot only be employed for the class of linear uncertain systems but also for nonlinear ones if they are reformulated in terms of quasi-linear state-space representations. However, naive polytopic uncertainty models may lead to quite conservative enclosures of the reachable states. Those, in turn, lead to conservative control strategies if the aforementioned interval enclosures are combined with strategies for the design of robust feedforward and feedback controllers. Therefore, this paper aims at the reduction of pessimism during interval-based state estimation by means of novel uncertainty models, relying on a parameter bounding approach that is implemented by means of a correlation analysis as well as a suitable principle axes transformation of the parameter space. The practical applicability of the proposed procedure is visualized for an experimentally validated thermal model of a solid oxide fuel cell stack, for which the computed interval bounds of reachable states represent a fundamental requirement for the design of a combined feedforward and feedback control allowing for preventing the violation of upper temperature limits in a guaranteed way.

Keywords: Solid oxide fuel cells, Interval analysis, Robust control, Convex optimization, Sensitivity analysis, LQR control method.

1. INTRODUCTION

Interval observers are characterized by the fact that they allow for estimating worst-case outer enclosures for those sets of state variables that are reachable for dynamic system models with bounded parameter uncertainty in the state and measurement equations. The same holds for bounded disturbances and noise in both, process and measurement models (Efimov et al., 2013; Chebotarev et al., 2015; Gouzé et al., 2000). Here, especially the class of cooperative systems (Smith, 2008) has attracted the interest of many researchers due to the fact that lower and upper state bounds can be computed independently after designing a Luenberger-like observer for both respective bounding systems (Rauh et al., 2018). Regardless whether the system models are given by crisp parameter values or by (in the linear case) system matrices which contain interval entries, this independence of lower and upper bounding systems can be ensured if the dynamics can be reformulated into a (quasi-)linear set of state equations in which the system matrix has a Metzler structure. Here, Metzler matrices are characterized by strictly non-negative entries on all off-diagonal elements (Kaczorek, 2002).

Such dynamic system models given in terms of Metzler matrices can be found in a wide range of applications from the domain of thermo-fluidic systems. As discussed, for example, in Rauh et al. (2018) in more detail, state estimation and temperature control for solid oxide fuel cells (SOFCs) belong to this class of applications. Despite the fact that a direct application of interval observer design procedures, such as those proposed by Efimov et al. (2013); Raïssi and Efimov (2018), leads to guaranteed outer estimates of all reachable states after a quasi-linear reformulation of the state equations, the classically applied polytopic uncertainty models have the drawback of producing state bounds that may be too pessimistic for the design of highly efficient feedforward and feedback control procedures.

For this reason, this paper aims at deriving a novel uncertainty description which allows for dealing with the following aspects:

- bounded uncertainty in selected system parameters,
- (polynomial) nonlinearities in the state equations which are overbounded by quasi-linear system models, and
- bounded external disturbances.

Here, the novelty of the proposed uncertainty modeling technique can be seen in a reduction of pessimism by capturing inter-relations between individual entries of the system matrices of the aforementioned quasi-linear models by determining the convex hull over representative submodels after a principal axes transformation of a generalized parameter vector. This principal axes transformation is employed to select extremal system models which result from finding guaranteed outer enclosures for the parameter ranges of all entries in state- and parameter-dependent system matrices. In combination with computationally efficient routines for finding a convex hull (Barber et al., 1996) over all extremal system models, it becomes possible to design not only interval observers with guaranteed cooperative error dynamics, but also feedback control procedures, stabilizing the corresponding closed-loop behavior in a guaranteed way. Besides the guaranteed robust stabilization, further goals such as minimizing the worst-case diameter of the intervals of expected tracking errors as well as a penalization of the required control effort can be achieved efficiently if robust H_2 design approaches are combined with the novel uncertain system representation.

Based on an underlying robust stabilization of the system dynamics, this paper presents an extension of the control structure by a sensitivity-based feedforward control. It allows for the development of an online predictive control strategy if it is implemented in a real-time framework.

This paper is structured as follows: Sec. 2 gives an overview of the control-oriented modeling of an SOFC stack which serves as the benchmark scenario for which the novel scheme for uncertainty modeling is derived in Sec. 3. Secs. 4 and 5 focus on the design and implementation of both, robust feedback controllers and sensitivity-based feedforward strategies, where the latter are motivated by a corresponding offline tracking control and learning-type feedback design published in Rauh et al. (2012). Finally, simulation results are given at the end of Sec. 5 before an outlook on future work concludes this paper in Sec. 6.

2. MODELING THE THERMAL BEHAVIOR OF SOFC STACK MODULES

The mathematical model of an SOFC can be split into its electro-chemical and its thermal behavior (Pukrushpan et al., 2005; Bove and Ubertini, 2008; Rauh et al., 2014), while this paper focuses on the latter. In general, the thermal behavior of an SOFC stack can be described by nonlinear partial differential equations, taking into account the non-homogeneous temperature distribution. Because of the challenges given by solving partial differential equations, the system is transformed into sets of ordinary differential equations (ODEs) for a control-oriented description. Assuming that the temperature distribution is piece-wise homogeneous, the whole stack is semi-discretised into a finite number of $n = L \cdot M \cdot N$ equally large cuboid elements by means of an early lumping approach (cf. Fig. 1).

To describe the temperature distribution, an energy balance

$$\dot{\vartheta}_{\mathcal{I}} = \frac{1}{c_{\mathcal{I}} m_{\mathcal{I}}} \left(\dot{Q}_{\text{HT}}^{\mathcal{I}} + \sum_{G \in \{\text{AG}, \text{CG}\}} \dot{Q}_{G, \mathcal{I}_j}^{\mathcal{I}} + \dot{Q}_{\text{EL}}^{\mathcal{I}} + \dot{Q}_{\text{R}}^{\mathcal{I}} \right) \quad (1)$$

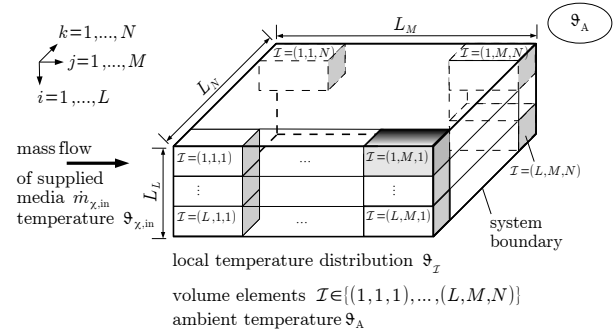


Fig. 1. Spatial semi-discretization of the fuel cell stack module.

is formulated for each finite volume element $\mathcal{I} := (i, j, k) \in \{(1, 1, 1), \dots, (L, M, N)\}$ with

- $\dot{Q}_{\text{HT}}^{\mathcal{I}}$: heat transfer due to heat conduction and convection (comprising a linearized model for heat radiation),
- $\sum_{G \in \{\text{AG}, \text{CG}\}} \dot{Q}_{G, \mathcal{I}_j}^{\mathcal{I}}$: enthalpy flows of the supplied gases, where χ in Fig. 1 denotes all relevant gas fractions at the anode and cathode side,
- $\dot{Q}_{\text{R}}^{\mathcal{I}}$: exothermic reaction enthalpies, and
- $\dot{Q}_{\text{EL}}^{\mathcal{I}}$: Ohmic losses due to electric currents $I_{\mathcal{I}}$.

Eq. (1) can be transformed into a quasi-linear state space representation

$$\dot{\mathbf{x}} = \mathbf{A}(\mathbf{x}, \mathbf{p}) \cdot \mathbf{x} + \mathbf{b}(\mathbf{x}, \mathbf{p}) \cdot u + \mathbf{Z}(\mathbf{x}, \mathbf{p}) \cdot \mathbf{e} \quad (2)$$

where the uncertainties lie in the parameter vector \mathbf{p} . State-dependent nonlinearities in $\mathbf{A}(\mathbf{x}, \mathbf{p})$, $\mathbf{b}(\mathbf{x}, \mathbf{p})$, and $\mathbf{Z}(\mathbf{x}, \mathbf{p})$ result from polynomial temperature dependencies of heat capacities as well as reaction enthalpies.

For this paper, one of the simplest, practically useful semi-discretizations is given by $L = N = 1$ with $M = 3$, whereby the SOFC stack temperature distribution is approximated in the direction of the parallel gas mass flows of both, the anode gas (i.e. the fuel gas mixture) and the cathode gas (typically preheated air).

For this case of $n = 3$ finite volume elements, the system matrix is defined by

$$\mathbf{A}(\mathbf{x}, \mathbf{p}) = \begin{bmatrix} a_{11} & a_{12} & 0 \\ a_{21} & a_{22} & a_{23} \\ 0 & a_{32} & a_{33} \end{bmatrix} \quad (3)$$

with the state vector of element temperatures

$$\mathbf{x} = [\vartheta_{(1,1,1)} \quad \vartheta_{(1,2,1)} \quad \vartheta_{(1,3,1)}]^T \quad (4)$$

For a pure temperature control for the heat-up phase, where $\dot{Q}_{\text{R}}^{\mathcal{I}} = 0$ and $\dot{Q}_{\text{EL}}^{\mathcal{I}} = 0$, the system input

$$u = \vartheta_{\text{CG}, \text{in}} \quad (5)$$

consists of the inlet temperature of the cathode gas $\vartheta_{\text{CG}, \text{in}}$ with the resulting input vector

$$\mathbf{b}(\mathbf{x}, \mathbf{p}) = [b_{11} \quad 0 \quad 0]^T \quad (6)$$

Previous work, cf. Rauh et al. (2014) and the references therein, performed an initial identification of the matrices (3) and (6) based on experimental data, whereby the interval-valued enclosure for $\mathbf{A}(\mathbf{x}, \mathbf{p})$ is strictly Metzler and the vector $\mathbf{b}(\mathbf{x}, \mathbf{p})$ is element-wise non-negative.

The ambient temperature ϑ_A and the inlet temperature of the anode gas $\vartheta_{AG,in}$ represent a measurable disturbance

$$\mathbf{e} = [\vartheta_A \ \vartheta_{AG,in}]^T \quad (7)$$

coupled with the system dynamics in terms of the disturbance input matrix

$$\mathbf{Z}(\mathbf{x}, \mathbf{p}) = \begin{bmatrix} z_{11} & z_{12} \\ z_{21} & 0 \\ z_{31} & 0 \end{bmatrix}. \quad (8)$$

For the reaction phase, where $\dot{Q}_R^T \neq 0$ and $\dot{Q}_{EL}^T \neq 0$, the thermal system model has to be extended according to Rauh et al. (2014) to account for the augmented disturbance input vector

$$\tilde{\mathbf{e}} = \left[\vartheta_A \ \vartheta_{AG,in} \ \frac{1}{3}I \right]^T \quad (9)$$

under the assumption of a homogeneous current distribution in the SOFC stack which is represented by $I_{(1,1,1)} = I_{(1,2,1)} = I_{(1,3,1)} = \frac{1}{3}I$ for a semi-discretization under investigation into three elements.

The outlet temperature $\vartheta_{(1,3,1)}$ denotes the output as in

$$y(t) = [0 \ 0 \ 1] \cdot \mathbf{x}(t). \quad (10)$$

In previous work, Ifqir et al. (2017); Rauh et al. (2018); Ifqir et al. (2019), it was considered that the individual uncertain entries in the system matrix $\mathbf{A}(\mathbf{x}, \mathbf{p})$ as well as in the input vector $\mathbf{b}(\mathbf{x}, \mathbf{p})$ are independent of each other. This leads to a conservative solution. For this work, a refined polytopic model is chosen, in consideration of the dependence between the entries in these matrices. Therefore, the state intervals are split into subboxes to build a tight convex hull after a principal axes transformation, so that nonlinearities and uncertainties are bounded rigorously with less overestimation. As a result, the control design becomes easier to perform. Especially, it provides enhanced possibilities for an optimization with respect to state constraints such as maximum admissible stack temperatures.

3. POLYTOPIC UNCERTAINTY REPRESENTATION WITH PRINCIPAL AXES TRANSFORMATION

In many practical applications, it is possible to describe the influence of uncertainty with a polytopic representation \mathcal{P} , where its vertex matrices yield a convex outer enclosure for all possible system matrices. Since these matrices typically depend on uncertain but bounded state or parameter intervals, it is common to use the extremal interval bounds to represent the polytope. As shown in Rauh and Kersten (2020), axes-parallel representations for the uncertainty, i.e., treating each of the matrix entries as independent, may lead to a blow-up of the estimated state enclosures in simulations or even to infeasible tasks of a robust controller synthesis due to the involved overapproximation of possible system models. Therefore, it is desired to reduce this conservatism by removing the independent consideration of parameter intervals by capturing their physical interrelations. This is accomplished by subdividing the range of possible operating conditions, which influence the terms $\mathbf{A}(\mathbf{x}, \mathbf{p})$, $\mathbf{b}(\mathbf{x}, \mathbf{p})$, and $\mathbf{Z}(\mathbf{x}, \mathbf{p})$, into N_L mutually disjoint subintervals

$$\left[\mathbf{x}^{(i,\xi)} \right] \in \left[\underline{\mathbf{x}}^{(i)}; \bar{\mathbf{x}}^{(i)} \right] \quad \text{with} \quad (11)$$

$i \in \{1, \dots, N_L\}$. The same is done for the parameter vector \mathbf{p} if the respective values are as well given by uncertain domains. Besides an interval evaluation of the system and input matrices, it is possible to determine accurate (however, not necessarily fully verified) approximations for the ranges of all matrix entries, if sampling points $\mathbf{x}^{(i,\xi)} \in \left[\mathbf{x}^{(i)} \right]$ with $\xi \in \{1, \dots, \Xi\}$ are used for the range evaluation. This sampling guarantees to cover the full ranges if the entries in the system and input matrices are monotonic with respect to these values. Then, using the respective interval endpoints is sufficient. Assuming that a point-wise evaluation of $\mathbf{A}(\mathbf{x}, \mathbf{p})$ and $\mathbf{b}(\mathbf{x}, \mathbf{p})$ has been performed to determine the possible operating conditions, all matrix (resp., vector) entries are transformed by a principal axes transformation for efficiently determined axes-parallel interval boxes enclosing uncertainties that show a dominant linear dependency.

Therefore, the entries in both $\mathbf{A}(\mathbf{x}, \mathbf{p})$ and $\mathbf{b}(\mathbf{x}, \mathbf{p})$ are evaluated along the operating points $\xi \in \{1, \dots, \Xi\}$ for each subinterval i and are summarized in a matrix

$$\mathbf{X}^{(i)} = \begin{bmatrix} a_{11}(\mathbf{x}^{(i,1)}, \mathbf{p}) & a_{11}(\mathbf{x}^{(i,2)}, \mathbf{p}) & \dots & a_{11}(\mathbf{x}^{(i,\Xi)}, \mathbf{p}) \\ \vdots & \vdots & \dots & \vdots \\ a_{33}(\mathbf{x}^{(i,1)}, \mathbf{p}) & a_{33}(\mathbf{x}^{(i,2)}, \mathbf{p}) & \dots & a_{33}(\mathbf{x}^{(i,\Xi)}, \mathbf{p}) \\ b_{11}(\mathbf{x}^{(i,1)}, \mathbf{p}) & b_{11}(\mathbf{x}^{(i,2)}, \mathbf{p}) & \dots & b_{11}(\mathbf{x}^{(i,\Xi)}, \mathbf{p}) \end{bmatrix}. \quad (12)$$

Furthermore, the matrix $\mathbf{X}^{(i)}$ is shifted into an offset-free form

$$\mathbf{D}^{(i)} = \mathbf{X}^{(i)} - \boldsymbol{\mu}^{(i)} \cdot [1 \dots 1] \quad (13)$$

by subtracting the mean values $\boldsymbol{\mu}^{(i)} \in \mathbb{R}^{n^2+n \times 1}$ of each row. A transformation matrix \mathbf{W} can then be determined either by a singular value decomposition of $\mathbf{D}^{(i)}$ or by the covariance matrix

$$\boldsymbol{\Sigma}^{(i)} = \frac{1}{\Xi-1} \mathbf{D}^{(i)} \cdot (\mathbf{D}^{(i)})^T. \quad (14)$$

Here, the transformation matrix \mathbf{W} is given by sorting the eigenvectors of $\boldsymbol{\Sigma}^{(i)}$ according to their largest eigenvalues and is used to transform the matrix $\mathbf{D}^{(i)}$ into the new coordinates

$$\mathbf{y}^{(i)} = \mathbf{W}^{-1} \mathbf{D}^{(i)}, \quad (15)$$

where $\mathbf{W}^{-1} = \mathbf{W}^T$ holds if all columns of \mathbf{W} are normalized to length one with all eigenvalues being strictly distinct. The lower and upper bounds are extracted according to $\mathcal{Y}_l^{(i)} \in \left[\underline{\mathcal{Y}}_l^{(i)}; \bar{\mathcal{Y}}_l^{(i)} \right]$ with

$$\underline{\mathcal{Y}}_l^{(i)} = \min_{\xi \in \{1, \dots, \Xi\}} \left(\mathcal{Y}_{l\xi}^{(i)} \right) \quad \text{and} \quad \bar{\mathcal{Y}}_l^{(i)} = \max_{\xi \in \{1, \dots, \Xi\}} \left(\mathcal{Y}_{l\xi}^{(i)} \right) \quad (16)$$

for each row l . To determine an axes-aligned subbox, all possible combinations of extremal bounds for each row of $\mathcal{Y}^{(i)}$ are used to define the vertices

$$\mathbf{y}^{(i)} = \left\{ \left[\begin{array}{c} \underline{\mathcal{Y}}_1^{(i)} \\ \underline{\mathcal{Y}}_2^{(i)} \\ \vdots \\ \underline{\mathcal{Y}}_{n^2+n}^{(i)} \end{array} \right], \left[\begin{array}{c} \bar{\mathcal{Y}}_1^{(i)} \\ \underline{\mathcal{Y}}_2^{(i)} \\ \vdots \\ \underline{\mathcal{Y}}_{n^2+n}^{(i)} \end{array} \right], \dots, \left[\begin{array}{c} \bar{\mathcal{Y}}_1^{(i)} \\ \bar{\mathcal{Y}}_2^{(i)} \\ \vdots \\ \bar{\mathcal{Y}}_{n^2+n}^{(i)} \end{array} \right] \right\}. \quad (17)$$

After a backward transformation of the extremal realizations collected in $\mathcal{Y}^{(i)}$ into the original coordinates according to

$$\mathcal{X}^{(i)} = \mathbf{W} \mathcal{Y}^{(i)} + \boldsymbol{\mu}, \quad (18)$$

a convex hull over all of these realizations with the resulting index set

$$\mathcal{P} = \text{convhulln}(\mathbf{x}^{(i)}, \dots, \mathbf{x}^{(N_L)}) \quad (19)$$

is determined using the quickhull algorithm implemented in MATLAB (Barber et al., 1996). This leads to a polytopic outer enclosure containing $n_{\mathcal{P}}$ vertices. Note that a complexity-reducing merging of subdomains becomes possible, if multiple submodels $\mathbf{X}^{(i)}$ are transformed with the help of an identical transformation matrix \mathbf{W} and if they are combined when determining the range bounds (16).

Exemplarily, Fig. 2 depicts the system matrix entries a_{22} and a_{33} for the SOFC model which exhibit a dominant linear dependence. Consequently, more conservative enclosures in terms of axes-parallel boxes as a common practice shown in red lead an excessively wide polytope, where the resulting number of vertices represented by green stars is also undesirably large ($n_{\mathcal{P}} = 19$). In comparison, the enclosure after the principal axes transformation described above leads to the ranges highlighted in Fig. 3. They are not only narrower but are typically also given by a smaller number of vertices ($n_{\mathcal{P}} = 10$).

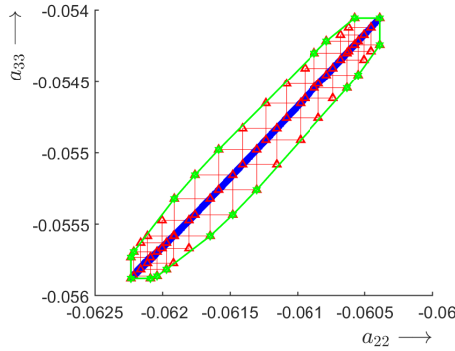


Fig. 2. Polytopic uncertainty model without principal axes transformation for $N_L = 9$.

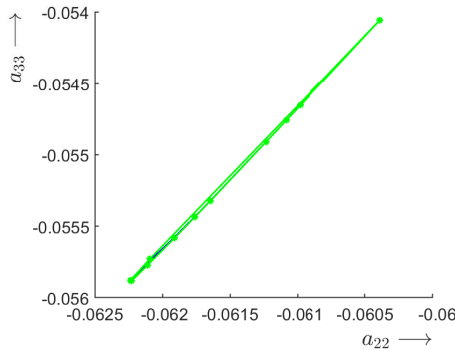


Fig. 3. Polytopic uncertainty model after a principal axes transformation for $N_L = 9$.

4. ROBUST FEEDBACK CONTROL DESIGN

The robust control strategy developed in this paper consists of a two-stage design. In the first step, an underlying robust linear state feedback is designed for the list of all vertex matrices $j \in \{1, \dots, n_{\mathcal{P}}\}$ resulting from the evaluation of (19) in the previous section. The respective controller

$$u(t) = -\mathbf{k}^T \mathbf{x}(t) + u_{ff}(t) \quad (20)$$

with the vertex-independent gain \mathbf{k}^T is extended in a second step (see Sec. 5) by a feedforward signal $u_{ff}(t)$

designed by using a sensitivity-based procedure to prevent overshooting maximum admissible stack temperatures.

Stability of the underlying linear feedback controller for the complete range of possible operating conditions is ensured if the gain vector \mathbf{k}^T satisfies the bilinear matrix inequality

$$(\mathbf{A}_j - \mathbf{b}_j \mathbf{k}^T)^T \cdot \mathbf{P} + \mathbf{P} \cdot (\mathbf{A}_j - \mathbf{b}_j \mathbf{k}^T) \prec 0 \quad (21)$$

with the yet unknown, positive-definite matrix $\mathbf{P} = \mathbf{P}^T \succ 0$ serving as the parameterization of a vertex-independent Lyapunov function candidate for the closed-loop dynamics. Applying the linearizing change of variables $\mathbf{Q} = \mathbf{P}^{-1} \succ 0$ and $\mathbf{Y} = \mathbf{k}^T \mathbf{P}^{-1}$, the inequality (21) is transformed into its linear equivalent form

$$\mathbf{A}_j \mathbf{Q} + \mathbf{Q} \mathbf{A}_j^T - \mathbf{b}_j \mathbf{Y} - \mathbf{Y}^T \mathbf{b}_j^T \prec 0. \quad (22)$$

In addition to stability of the closed-loop dynamics, optimality properties such as the minimization of the H_2 norm between disturbance inputs and system output(s) can be included if the LMI (22) is extended according to

$$\begin{bmatrix} \mathbf{A}_j \mathbf{Q} + \mathbf{Q} \mathbf{A}_j^T - \mathbf{b}_j \mathbf{Y} - \mathbf{Y}^T \mathbf{b}_j^T & \mathbf{Z} \\ \mathbf{Z}^T & -\mathbf{I} \end{bmatrix} \prec 0, \quad (23)$$

where the matrix \mathbf{Z} represents a point-valued representation of the disturbance input (or in case of non-negligible uncertainty, corresponding polytope vertices which then need to be included in (12)). Optimality of the gain \mathbf{k}^T results from a minimization of the trace of the symmetric, positive-definite auxiliary matrix Φ according to

$$\min\{\text{trace}\{\Phi\}\} \quad \text{satisfying} \quad \begin{bmatrix} \mathbf{Q} & \mathbf{Q} \mathbf{c} \\ \mathbf{c}^T \mathbf{Q} & \Phi \end{bmatrix} \succ 0, \quad (24)$$

which is further extended by a restriction that enforces purely real eigenvalues of the closed-loop system (Scherer and Weiland, 2011).

Using this information, the nonlinear closed-loop dynamics are given by the differential equations

$$\dot{\mathbf{x}} = \mathbf{A}_C(\mathbf{x}, \mathbf{p}) \cdot \mathbf{x} + \mathbf{b}(\mathbf{x}, \mathbf{p}) \cdot u_{ff} + \mathbf{Z}(\mathbf{x}, \mathbf{p}) \cdot \mathbf{e} \quad (25)$$

with $\mathbf{A}_C(\mathbf{x}, \mathbf{p}) = \mathbf{A}(\mathbf{x}, \mathbf{p}) - \mathbf{k}^T \cdot \mathbf{b}(\mathbf{x}, \mathbf{p})$. Unfortunately, the solution of the optimization problem described above typically leads to controller gains \mathbf{k}^T which violate the structural Metzler properties of the closed-loop system matrix $\mathbf{A}_C(\mathbf{x}, \mathbf{p})$. Hence, forecasting worst-case bounds for all possible system states is not directly possible by simulating lower and upper bounding systems for the state trajectories as it was done, for example, in Rauh et al. (2018); Rauh and Kersten (2020). To avoid the introduction of structural restrictions on the ranges for the gain values \mathbf{k}^T (typically leading to suboptimal control parameterizations) a similarity transformation according to Kersten et al. (2018) on the closed-loop state equations (25) is performed according to Fig. 4. This transformation yields an equivalent system representation ensured to be cooperative due to the Metzler matrix $\tilde{\mathbf{A}}_C$ so that lower and upper state bounds can be forecasted independently as shown, for example, in Efimov et al. (2013).

5. SENSITIVITY-BASED FEEDFORWARD OPTIMIZATION AND NUMERICAL VALIDATION OF THE ROBUST FEEDBACK CONTROLLER

As mentioned in Sec. 4, the feedforward control signal $u_{ff}(t)$ is computed by a sensitivity-based approach. For

Set $i := 1$
While $i \leq N_L$ with $i = \{1, 2, \dots\}$
Determine $[\mathbf{A}_C]^{(i)} = [\underline{\mathbf{A}}_C^{(i)}; \overline{\mathbf{A}}_C^{(i)}]$
Initialize eigenvalues $\lambda_0^{(i)}$ and eigenvector $\mathbf{T}_0^{(i)}$ with $\mathbf{eig}(\text{mid}([\mathbf{A}_C]^{(i)}))$
Determine the enclosures of the eigenvalues $[\lambda]^{(i)}$ and eigenvectors $[\mathbf{T}]^{(i)}$ with the INTLAB routine <code>verifyeig()</code>
Update $[\tilde{\lambda}] = \text{hull}([\tilde{\lambda}], [\lambda]^{(i)}); [\tilde{\mathbf{T}}] = \text{hull}([\tilde{\mathbf{T}}], [\mathbf{T}]^{(i)})$
Output $[\tilde{\mathbf{A}}_C] = \text{diag}([\tilde{\lambda}]) \quad [\tilde{\mathbf{b}}] = [\tilde{\mathbf{T}}]^{-1} \cdot [\mathbf{b}]$ $[\tilde{\mathbf{Z}}] = [\tilde{\mathbf{T}}]^{-1} \cdot [\mathbf{Z}] \quad [\tilde{\mathbf{c}}]^T = \mathbf{c}^T \cdot [\tilde{\mathbf{T}}]$

Fig. 4. Similarity transformation of the state equations.

that purpose, the cost function

$$J = \sum_{k=\tau}^{\tau+N_\tau} \mathcal{E}(t_k) \quad \text{with} \quad (26)$$

$$\mathcal{E}(t_k) = \underbrace{\frac{1}{2} \eta \cdot \left(y_d(t_k) - \frac{1}{2} \cdot \left(\bar{\vartheta}_{(1,3,1)}(t_k) + \underline{\vartheta}_{(1,3,1)}(t_k) \right) \right)^2}_{\mathcal{E}_1} + \underbrace{\frac{1}{2} \cdot \max(\bar{\vartheta}_{(1,3,1)}(t_i) - \vartheta_{\max}, 0)^2}_{\mathcal{E}_2} \quad (27)$$

and the reference trajectory $y_d(t_i)$ for the midpoint of the interval enclosure of the stack outlet temperature $\vartheta_{(1,3,1)}$ is minimized. Here, techniques for algorithmic differentiation are employed, which relate the differential $\frac{\partial J}{\partial \xi_i}$ of the cost function to the differential sensitivities

$$\mathbf{s}_i(t) := \frac{\partial \mathbf{x}(t)}{\partial \xi_i} \in \mathbb{R}^{n_x} \quad (28)$$

of the state equations $\dot{\mathbf{x}} = \mathbf{f}(\mathbf{x}(t), \xi)$. These sensitivities can be computed by solving appropriate initial value problems to the ordinary differential equations

$$\dot{\mathbf{s}}_i(t) = \frac{\partial \mathbf{f}(\mathbf{x}(t), \xi)}{\partial \mathbf{x}} \cdot \mathbf{s}_i(t) + \frac{\partial \mathbf{f}(\mathbf{x}(t), \xi)}{\partial \xi_i}, \quad (29)$$

where the vector components ξ_i contain all parameters to be adjusted during the feedforward control design.

For a pure offline solution, ξ is equal to a time-invariant feedforward gain S according to $u_{\text{ff}}(t) = S \cdot y_d(t)$, which is adapted iteratively according to

$$S_\kappa = S_{\kappa-1} + \Delta S_\kappa \quad (30)$$

with the increment

$$\Delta S_\kappa = - \left(\frac{\partial J(S_{\kappa-1} + \Delta S_\kappa)}{\partial \Delta S_\kappa} \Big|_{\Delta S_\kappa=0} \right)^+ \cdot J(S_{\kappa-1}) \quad (31)$$

This increment is chosen in such a way that the zero of the linearized cost function

$$J(S_{\kappa-1} + \Delta S_\kappa) \approx J(S_{\kappa-1}) + \frac{\partial J(S_{\kappa-1} + \Delta S_\kappa)}{\partial \Delta S_\kappa} \Big|_{\Delta S_\kappa=0} \cdot \Delta S_\kappa \quad (32)$$

is determined in each step.

Setting the weight η in the term \mathcal{E}_1 of the cost function (26) with (27) to a sufficiently small value allows for a guaranteed prevention of overshooting a pre-defined upper temperature bound. The result, including the feedback gain from the previous section together with the prediction of the output intervals after the similarity transformation in Fig. 4 is shown in Fig. 5. In addition, Fig. 6 demonstrates the convergence of the sensitivity-based optimization within less than 10 iterations if $S_{\kappa=0} = 0$ is chosen.

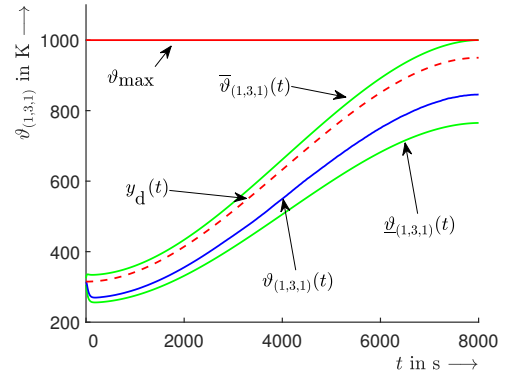


Fig. 5. Offline optimization with a time-invariant feedforward gain S .

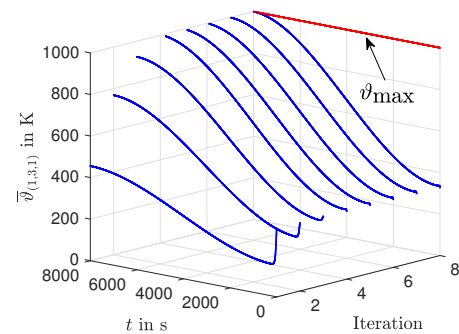


Fig. 6. Iterative optimization of the constant gain S .

A generalization — on the basis of an online optimization of sequences of $N_\tau = 10$ piecewise constant gains — valid for a duration of 2s each, from which only the first one is applied to the system, significantly improves the tracking accuracy of the desired output in Fig. 7. For the beginning of each temporally moving prediction window, state estimates according to Rauh et al. (2018) are required. Note, a numerical experiment with adapting the feedforward gains only each tenth second lead to practically identical results, however, with a significant reduction of the computational effort. The overall structure of the robust feedback controller including the sensitivity-based optimization is depicted in Fig. 8 as a block diagram.

6. CONCLUSIONS AND FUTURE WORK

In this paper, a robust closed-loop control strategy was derived on the basis of a novel polytopic uncertainty model, which results from a control-oriented modeling of a high-temperature SOFC stack. With the help of LMIs, a robust feedback controller was designed so that an H_2 -motivated cost function was minimized. However, this controller typically leads to a loss of cooperativity of the underlying

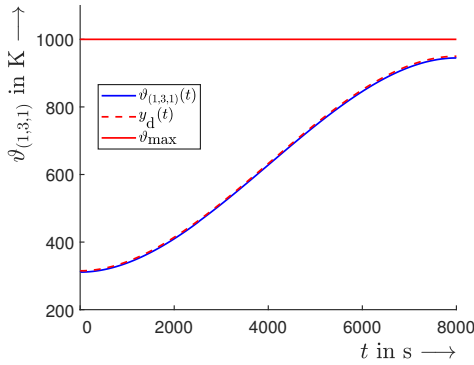


Fig. 7. Online optimization with time-varying feedforward gains $S(t_\tau)$, $t_\tau \in \{2, 4, 6, \dots\}$ s.

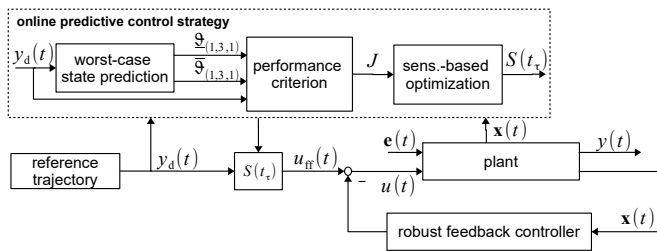


Fig. 8. Block diagram of the robust control structure.

closed-loop control system. To recover the possibility for a simple independent forecast of lower and upper bounds on the system output, this control strategy is interfaced with a state-space transformation. In such a way, an offline feedforward control synthesis as well as a sensitivity-based predictive control procedure were implemented which make sure that neither of the worst-case state trajectories violates predefined system constraints, for example the upper threshold on the admissible temperature.

In future work, the robust controller should be implemented at a test rig for experimental validation. Furthermore, the underlying robust state feedback can be generalized to an adaptive scheme with state-dependent gain values to improve the control accuracy while still being compatible with hard state constraints. Although this paper was focused purely on the heating phase of the SOFC, the presented controller can be generalized directly to the reaction phase. There, exothermal reaction enthalpies lead to bounded disturbances from the temperature control point of view, leading to the necessity to firstly determine the stack segment \mathcal{I} with the maximum temperature $y = \arg \max_{\mathcal{I}} \{\vartheta_{\mathcal{I}}(t)\}$ for which the predictive controller has to make sure that upper thresholds are not violated, cf. Rauh et al. (2014).

REFERENCES

Barber, C., Dobkin, D., and Huhdanpaa, H. (1996). The Quickhull Algorithm for Convex Hulls. *ACM Transactions on Mathematical Software*, 22(4), 469–483.

Bove, R. and Ubertini, S. (eds.) (2008). *Modeling Solid Oxide Fuel Cells*. Springer, Berlin.

Chebotarev, S., Efimov, D., Raïssi, T., and Zolghadri, A. (2015). Interval Observers for Continuous-Time LPV Systems with L1/L2 Performance. *Automatica*, 58, 82–89.

Efimov, D., Raïssi, T., Chebotarev, S., and Zolghadri, A. (2013). Interval State Observer for Nonlinear Time Varying Systems. *Automatica*, 49(1), 200–205.

Gouzé, J.L., Rapaport, A., and Hadj-Sadok, M.Z. (2000). Interval Observers for Uncertain Biological Systems. *Ecological modelling*, 133(1), 45–56.

Ifqir, S., Rauh, A., Kersten, J., Ichalal, D., Ait-Oufroukh, N., and Mammam, S. (2019). Interval Observer-Based Controller Design for Systems with State Constraints: Application to Solid Oxide Fuel Cells Stacks. In *IEEE Intl. Conference on Methods and Models in Automation and Robotics MMAR 2019*. Miedzyzdroje, Poland.

Ifqir, S., Ait-Oufroukh, N., Ichalal, D., and Mammam, S. (2017). Synchronous interval observer design for switched lpv systems using multiple quadratic isslyapunov functions. In *25th Mediterranean Conference on Control and Automation (MED)*, 388–393. IEEE.

Kaczorek, T. (2002). *Positive 1D and 2D Systems*. Springer-Verlag, London.

Kersten, J., Rauh, A., and Aschemann, H. (2018). State-Space Transformations of Uncertain Systems with Purely Real and Conjugate-Complex Eigenvalues into a Cooperative Form. In *IEEE Intl. Conference on Methods and Models in Automation and Robotics MMAR 2018*. Miedzyzdroje, Poland.

Pukrushpan, J., Stefanopoulou, A., and Peng, H. (2005). *Control of Fuel Cell Power Systems: Principles, Modeling, Analysis and Feedback Design*. Springer, Berlin, 2nd edition.

Raïssi, T. and Efimov, D. (2018). Some Recent Results on the Design and Implementation of Interval Observers for Uncertain Systems. *at-Automatisierungstechnik*, 66(3), 213–224.

Rauh, A., Kersten, J., and Aschemann, H. (2018). An Interval Observer Approach for the Online Temperature Estimation in Solid Oxide Fuel Cell Stacks. In *Proc. of the 16th European Control Conference (ECC)*, 1596–1601. IEEE, Limassol, Cyprus.

Rauh, A., Krägenbring, O., Pröhl, L., and Aschemann, H. (2012). Sensitivity-Based Approaches for an Efficient Design of Learning-Type Controllers of a Flexible High-Speed Rack Feeder System. In *Proceedings of IEEE Multi-Conference on Systems and Control*. Antibes, France.

Rauh, A., Senkel, L., Kersten, J., and Aschemann, H. (2014). Reliable Control of High-Temperature Fuel Cell Systems Using Interval-Based Sliding Mode Techniques. *IMA Journal of Mathematical Control and Information*, 33(2), 457–484.

Rauh, A. and Kersten, J. (2020). From Verified Parameter Identification to the Design of Interval Observers and Cooperativity-Preserving Controllers — An Experimental Case Study. *Acta Cybernetica*. In print.

Scherer, C. and Weiland, S. (2011). Linear Matrix Inequalities in Control. In W.S. Levine (ed.), *Control System Advanced Methods*, The Electrical Engineering Handbook Series, 24–1—24–30. CRC Press, Boca Raton, 2nd edition.

Smith, H. (2008). *Monotone Dynamical Systems: An Introduction to the Theory of Competitive and Cooperative Systems*. 41. American Mathematical Soc.